A Dual-Circularly Polarized and Flexible Metasurface Antenna Based on Graphene Assembled Film for Satellite Communications

Journal:	*ACS Applied Materials & Interfaces*
Manuscript ID	am-2024-01211w.R1
Manuscript Type:	Article
Date Submitted by the Author:	08-Mar-2024
Complete List of Authors:	Luo, Zhi; Hubei Engineering Research Center of RF-Microwave Technology and Application, Wuhan University of Technology, Wuhan 430070, China Li, Peng; Hubei Engineering Research Center of RF-Microwave Technology and Application, Wuhan University of Technology, Wuhan 430070, China Xin, Yitong; Hubei Engineering Research Center of RF-Microwave Technology and Application, Wuhan University of Technology, Qian, Wei; Wuhan University of Technology Zhou, Bilei; Air Force Early Warning Academy, Wuhan 430019, China Song, Rongguo; Wuhan University of Technology Zu, Haoran; Wuhan University of Technology School of Information Engineering Shen, Jie; Wuhan University of Technology He, Daping; Wuhan University of Technology, State Key Laboratory of Advanced Technology for Materials Synthesis and Processing

A Dual-Circularly Polarized and Flexible Metasurface Antenna Based on Graphene Assembled Film for Satellite Communications

Zhi Luo[a‡], *Peng Li*[a‡], *Yitong Xin*[a], *Wei Qian*[a], *Bilei Zhou*[b], *Rongguo Song*[a,b], *Haoran Zu*[a,c,*], *Jie Shen*[a,*], *Daping He*[a,*]

[a] Hubei Engineering Research Center of RF-Microwave Technology and Application, Wuhan University of Technology, Wuhan 430070, China

[b] Air Force Early Warning Academy, Wuhan 430019, China

[c] School of Information Engineering, Wuhan University of Technology, Wuhan 430070, China

‡ These authors contributed equally to this work
* Corresponding author

E-mail addresses: zuhr@whut.edu.cn
E-mail addresses: shenjie@whut.edu.cn
E-mail addresses: hedaping@whut.edu.cn

Abstract

Traditional metal materials used in electronic devices are often problematic due to issues like bending resistance, oxidation leading to failure and environmental pollution. To address these challenges, microwave electronic devices are constantly casting around for metal substitute materials with additional characteristics such as flexible, anti-corrosive and eco-friendly. However, finding suitable materials that are accessible for radio-frequency (RF) applications is a difficult yet promising task. Consequently, a high-performance metasurface antenna based on highly conductive graphene films for satellite communications is developed in this paper. The proposed graphene assembled films (GAFs) have a conductivity of up to 1.13×10^6 S/m. Simulation and measurement results confirm the excellent performance of the designed antenna. Comparative experiments are also conducted on salt spray and mechanical bending between GAF antenna patterns and copper foil counterparts, further demonstrating the outstanding flexible property and corrosion resistance performance of the prepared GAF.

Key Words: Graphene assembled film, metasurface antenna, flexibility, dual-circular polarization, satellite communication

1. Introduction

Over the past several decades, the continuous advancements of RF technology and microwave electronics, particularly the application of satellite communication (SatCom) in the fields of environmental monitoring and observation [1, 2], aerospace engineering [3, 4], disaster early warning and rescue disposition [5, 6], have made contributions to the progress of society. In order to diminish material loss and transfer RF energy to free space effectively, traditional forms of antennas and RF devices are generally manufactured in metal materials [7-9]. Nevertheless, confronted with the severe operating conditions, electrochemical corrosion caused by the interaction between the metals on

SatCom antennas and high air humidity and severe salt spray atmospheric environment poses an ordeal to the antenna's performance [10, 11]. In addition, the production and application of metals not only lead to the emission of a large number of pollutants but also increase the pressure on biological and ecological environments with each passing day, posing a threat to sustainable development [14-16]. With the growing desire for advanced high-conductivity metal substitute materials, numerous innovative materials have been developed for RF devices, such as graphene [17, 18], carbon nanotubes [19, 20], MXene [21, 22], Polypyrrole [23], etc. Moreover, these creative materials are physically satisfied with the characteristics of lightweight, flexible, and corrosion-resistant properties. RF and microwave applications proliferated therefrom [24-27].

The conductivity of conductive materials is a crucial factor in determining their effectiveness in electrical applications [28]. However, improving the conductivity of a material that is suitable for microwave devices while maintaining its mechanical strength poses a very challenging task. Graphene, due to its high conductivity, environmental friendliness, and excellent chemical stability, has gained widespread popularity in the field of RF electronic manufacturing [29-31]. Typically, for the sake of reducing the surface impedance of microwave devices so that capable of RF applications, conductive materials need to be thicker than a certain thickness to meet the requirement of skin depth [32]. New studies have delved into the close correlation between the electrical performance and conductivity of graphene films (GFs). The findings indicate that GFs with a conductivity of exceeding 10^6 S/m exhibit comparable conductor loss to cooper foil in the microwave band and millimetre-wave (mmWave) band, confirming that GFs meet the necessary conditions of RF microwave devices below this level of conductivity [33].

Circularly polarized (CP) antennas have been proven to effectively reduce multipath distortion and polarization mismatch, thus maintaining stable connections between transmitting and receiving antennas [34]. Furthermore, they are extensively utilized in SatCom, aerospace, and Global Navigation Satellite System (GNSS) due to their advantages of low-profile design and ease of fabrication. Meanwhile, metasurface technology utilizes artificially arranged periodic electromagnetic (EM) media to effectively manipulate EM waves for various applications [35]. Breakthroughs of metamaterials in various fields are emerging as an endless stream, such as spoof surface plasmon polaritons (SSPPs) [36], ceramic - based dielectric metamaterials [37], and the introduction of artificial intelligent (AI) algorithms into the design of metamaterials - based photonic devices [38]. As a low-cost antenna system scenario, metasurface antennas (MSAs) are gifted with wider frequency band coverage and lower profile than traditional multi-band patch antennas, accordingly enhancing the communication capacity of the SatCom systems and efficaciously dwindling their complexity.

In this paper, we investigate a dual-circular polarization (dual-CP) metasurface antenna of GAFs, specifically designed for SatCom scenarios with L-band operating frequency bands. By utilizing large-scale graphene oxide (LGO) nanosheets, the GAF is prepared with a conductivity of 1.13×10^6 S/m, which satisfies the demand of RF devices in the microwave band. Meanwhile, the thickness of GAFs is 27 μm, which also meets the necessity of skin depth for L-band RF signals. The GAF-based dual-CP metasurface antenna performs exceptionally well, according to both simulation and measurement results. Comparative experimentations on the bending resistance characteristics between GAF-based antenna patterns and copper-based antenna patterns are also conducted. The results indicated that GAF-based antennas maintain acceptable performance even after bending more than 50,000 times, while copper-based antennas show cracks or even complete fractures for a thousand bends. Additionally, to study the corrosion resistance of GAFs in a high salt spray environment, GAF-based and copper-based antennas are subjected to spray treatments (with an hour between each spray disposition). The GAF-based patterns maintained favourable electrical behaviour as before after twenty days passed by, whereas copper antennas are significantly corroded after just five days of salt spray disposition. This research manifests that GAF materials are capable of manufacturing high-performance RF electronic devices, with GAF-based antennas proving better flexibility, corrosion resistance, and mechanical resilient characteristics than copper-based antennas.

2. Experimental

2.1 Fabrication of GAF

To produce GAFs, a process involving centrifuging graphene oxide (GO) nanosheets is necessary. Large-scale graphene oxide nanosheet suspensions were obtained in this way, which are the precursors of preparing GAFs. Subsequently, due to the hydrophilicity of GO, numerous LGO nanosheets in the dispersion spontaneously stacked tightly into multilayer structures through hydrogen bonding. Then, the obtained LGO assembly film was placed in a high-temperature atmosphere furnace in an argon, carbonized at 1300° Celsius for 2 hours, and then subjected to graphitization treatment at 2850° Celsius for an hour. Finally, the reduced graphene film was rolled and pressed under 300 MPa of pressure to achieve the final GAF production.

2.2 Fabrication and measurement of GAF antenna

Above all, patterns on different layers of the antenna were obtained by cutting GAFs into preset structures with a laser engraving machine (LPKF Protolaser U4). It should be noted that the production of GAF-based patterns requires a reasonable adjustment of parameters such as the power of the laser, processing step speed, and the size of each processing area. Also, it is necessary to consider the processing and assembly methods of the antenna in antenna design to prevent potential problems in prototype fabricating. Then, the Epoxy Resin Adhesive (ERA) was employed to bond distinct layers of GAF structures with several supple Polydimethylsiloxane (PDMS) substrates successively to form the proposed antenna. Finally, a dispersion of silver nanoparticles and mucilage (Double-bond Chemical DB 2013) was used to form a secure and effective electrical attachment between the GAF-based feeding lines and SMA connectors.

The dual-CP metasurface antenna was measured by a vector network analyzer (VNA, Keysight N5247A) and a full-wave microwave anechoic chamber. One of the SMA connectors on the fabricated antenna was attached to a coaxial cable line, and the other counterpart was connected to a 50-ohm matching load to measure the transmission coefficient. The radiation patterns, axial ratio and realized gain of the GAF antenna were measured by resorting to the antenna far-field measurement system and VNA using a reference given gain horn antenna.

2.3 Materials characterization

The X-ray diffractometer (XRD) patterns were carried out by utilizing a Bruker D8 Advance diffractometer. The Raman spectra were recorded utilizing a LabRam HR Evolution Confocal laser Raman instrument (through Cu Kα radiation, $\lambda = 1.5406$ Å). Additionally, the morphology and microstructure images of GAF samples were acquired by employing a scanning electron microscope (SEM, ZEISS Gemini electron microscopy 300) and a high-resolution transmission electron microscope (HRTEM, JEM-2100F).

3. Results and discussion

3.1 Characterization of GAF

The digital photo of GAF, as depicted in Figure 1, showcases its exceptional flexibility and ability to be rolled into rolls. The surface SEM image (Figure 1b) reveals a smooth and crack-free surface of GAF without any visible holes. In Figure 1c, the cross-sectional SEM image confirms the thickness of GAF to be 27 um with tightly stacked graphene sheets. XRD pattern demonstrates a sharp and intense diffraction peak for GAF, including a well-defined graphite peak at approximately 26.5° indicating a high graphitization degree and an interlayer spacing (002) of about 0.34 nm, as illustrated in Figure 1d. The Raman spectra of GAF are presented in Figure 1e, where the almost disappearance of the D peak at around 1350 cm^{-1} indicates defects and disorder carbon are effectively restored. Additionally, fitting analysis on the 2D peaks suggests a high content of AB-stacking within GAF, further confirming its superior level of graphitization (Figure 1f). HRTEM images (Figure 1g and 1h) captured from the defoliated graphene sheet, clearly reveal continuous lattice fringes with an average of 0.34 nm are observed (Figure 1i), which is consistent with the XRD result.

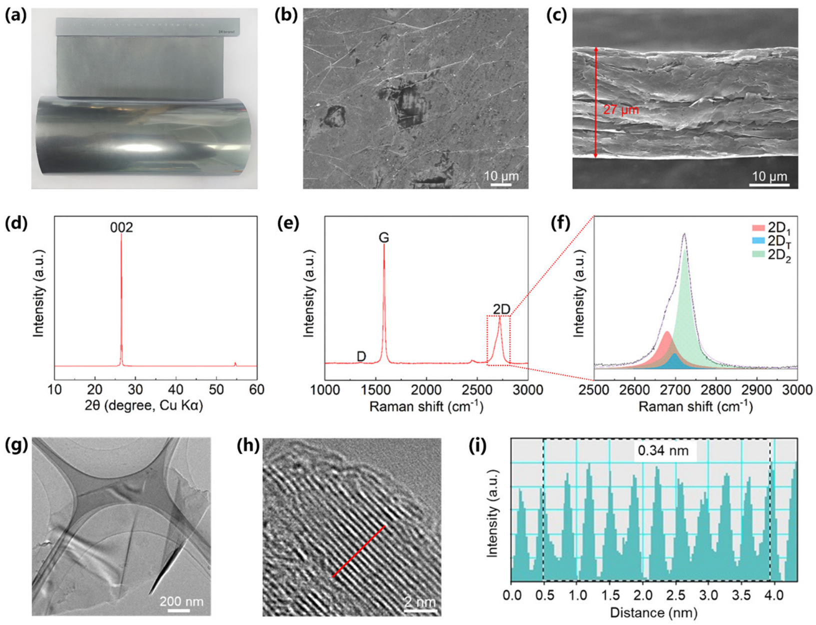

Figure 1. Characterization of GAFs. (a) The digital photo of GAF. (b) and (c) The surface and cross-section SEM images of GAF. (d) XRD pattern of GAF. (e) Raman spectra of GAF. (f) Fitting of the 2D peaks of GAF in Figure 1e. (g) and (h) HRTEM images at different magnifications of GAF. (i) The intensity profile along the red line in Figure 1h.

3.2 Antenna design and working principles

The exploded view of the proposed dual-CP metasurface antenna is showcased in Figure 2a. Comprised of several components, including an upper metasurface patch, a bottom microstrip feeding, sequentially rotating slot-lines, microstrip low-pass filter (LPF) and split-ring resonator (SRR) structures, each individual element is detailed in Figure 2b-d, respectively. The overall size of the designed antenna is 200 × 200 × 4.075 mm^3, PDMS with a relative permittivity of 2.7 and a dissipation factor of 0.02 are selected as the substrates. The conductive layer is fashioned from high conductivity GAFs, with a thickness of 27 μm.

Specifically, the metasurface consists of a 4 × 4 square patch with a side length of w_p and an equal clearance width of g are attached to the top substrate with a thickness of h_1, and four corner patches are chamfered in a width c. The introduction of these chamferings is to improve the axial ratio bandwidth, as shown in Figure S1. Two sets of orthogonal slot-lines are introduced sequentially by an annular microstrip line. These four crossed slot-lines have identical width s and varying lengths of l_1, l_2, l_3 and l_4, and the well symmetry is to preferably excite the top metasurface. The EM energy is then coupled from the near-field radiation of the slot-lines to the metasurface patches, resulting in a beam into free space. Through this way, a satisfactory CP performance is produced. With a thickness of h_2, the bottom substrate features a mirror-symmetric microstrip line that employs a two-terminal feeding modality. In addition, to eliminate any high-frequency interference signals, a fan-shaped five-order Butterworth step impedance LPF is introduced, while the SRR structure generates a radiation null at a lower frequency. The effect of introducing frequency-selective (FR) structures is depicted in Figure S2, the loading of the SRR structure into the proposed antenna induces a radiation null at the frequency of 1.1 GHz, while the LPF structure provides a deeper suppression at higher frequencies. All the specific values of the optimized parameter are annotated in Figure 2 and given in Table 1.

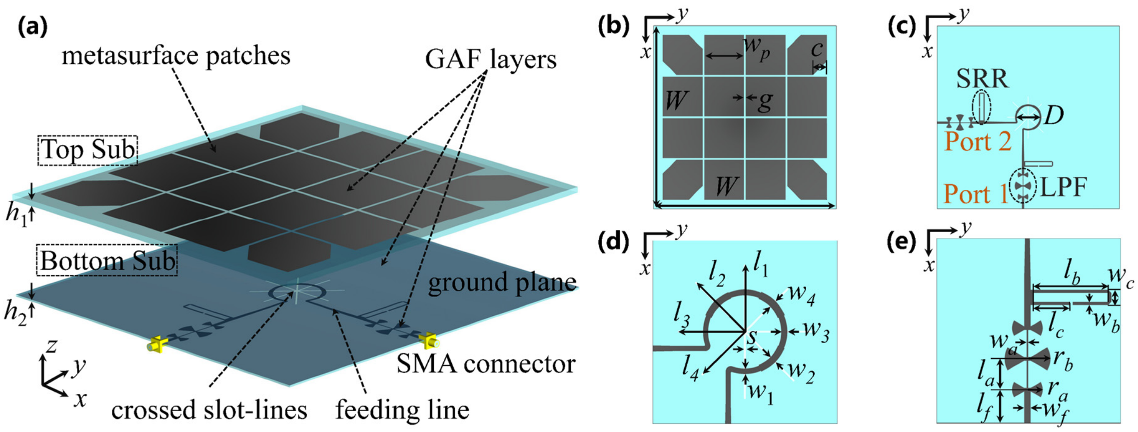

Figure 2. Configuration of the proposed dual-CP metasurface antenna. (a) Exploded 3-D view. (b) Top view. (c) Bottom view. (d) Geometry of the crossed sequential rotation slot-lines. (e) Structures of the LPF and SRR.

Table 1. Parameters of the proposed GAF antenna

Parameters	W	w_p	g	c	s	l_1	l_2
Values (mm)	200	43.5	0.5	15	0.5	23	24
Parameters	l_3	l_4	l_f	w_f	w_1	w_2	w_3
Values (mm)	23	24	21	2.6	1.8	2.4	2
Parameters	w_4	r_a	r_b	l_a	l_b	l_c	w_a
Values (mm)	2.6	6	9	12	31.6	16	0.7
Parameters	w_b	w_c	h_1	h_2	D		
Values (mm)	1.2	6	3	1	27		

To demonstrate the CP traits, we activated Port 1 and Port 2 is matched with a load. The surface current distributions of the simulated metasurface antenna are visualized at different phase points in Figure 3a-d. It is prominently apparent that the total current direction rotates 90° for every quarter cycle and the overall current movement displays a clockwise rotation, thus achieving left-handed circularly polarized radiation. The polarization characteristics of the designed antenna can be easily shifted to right-handed circular polarization (RHCP) by flipping the feeding approach.

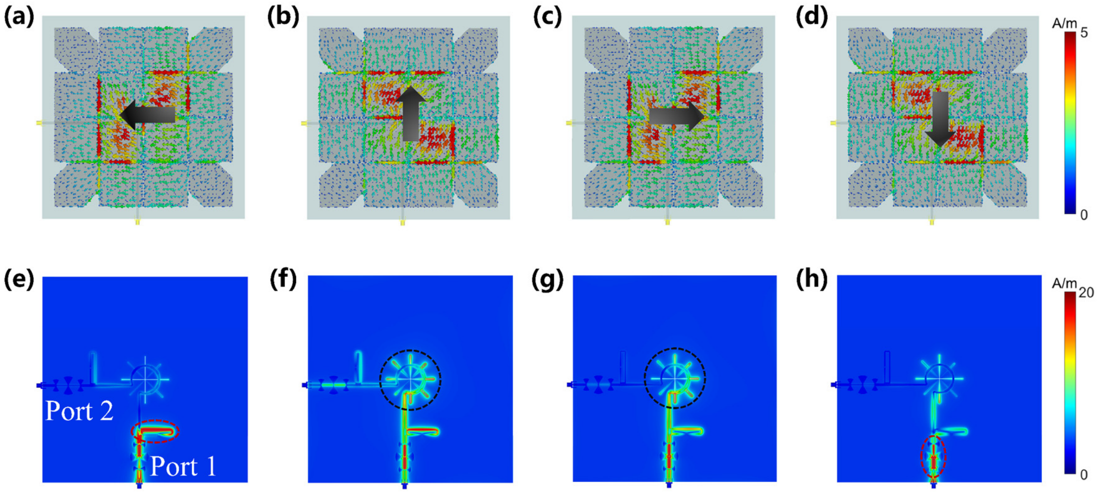

Figure 3. Current distributions of the metasurface patches at 1.6 GHz for successively increased phase values (Port 1 excited, Port 2 load matched). (a) 0°. (b) 90°. (c) 180°. (d) 270°., and maximum current distributions of the microstrip feeding line and its reference ground plane with crossed slot-lines at different frequency values. (e) 1.0 GHz. (f)1.5 GHz. (g) 1.7 GHz. (h) 2.2 GHz.

Circularly polarized radiation of the metasurface is inseparable from a carefully designed exciting network. The maximum current distributions of frequency points within the operating band at 1.5 GHz and 1.7 GHz, and out-of-band frequency points at 1.0 GHz and 2.2 GHz of the optimized feeding structure are depicted in Figure 3e-h. It is obvious that the SRR structure marked with a red circle on the side of the excited port resonated at 1.0 GHz from Figure 3e, there is a conspicuously large amount of EM energy concentration. Thus blocked the passage of EM signals at the corresponding frequency. Conversely, at frequencies of 1.5 GHz and 1.7 GHz, the current enters from Port 1 and couples to the slot-lines, with minimal current leakage to Port 2 due to excellent matching between the microstrip and crossed slots, thus the EM energy perfectly and effectively transmitted from the microstrip line to the next target structure within the black markings, as illustrated in Figure 3f, g. Furthermore, the current distribution at 2.2 GHz is described in Figure 3h, the EM energy is converged on the LPF structure and is incompetent to reach the vicinity of the annular feeding line (as shown in the dashed red circle). The current distributions demonstrate that the LPF and SRR structures are capable of maintaining the antenna's performance at the desired operating frequency range while also mitigating out-of-band interference.

3.3 Measurement results and analysis

The structures of the GAF-based antenna prototype, flexible characteristics representation, measurement environment, simulated and measured results are shown in Figure 4 and accompanying electronic supplementary materials. In Figure 4a, the GAF-based metasurface and feeding mirror-symmetric microstrip line are depicted, while Figure S3 displays the GAF ground bonded to the PDMS substrate. Proving the GAF patterns and dielectric substrate composite very well, their surface is considerably glossy and smooth, with a metallic lustre. Even after bonding GAF patterns onto PDMS films, their favourable flexibility is preserved. The metasurface, along with its PDMS substrate, can be bent to a 90° angle with ease, as sketched in Figure 4c, Figure S4 and Figure S5. Additionally, the thinner microstrip feeding part can even curl to a roll state. Despite being subjected to larger angles and minor radii of bending, GAF does not exhibit apparent any blistering and wrinkling.

The multi-probe dual-polarization antenna measurement system is shown in Figure 4d and Figure S6. The entire system encompasses a VNA and a microwave anechoic chamber. The antenna under test (AUT) is loaded at the centre of the platform and fixed with several paper tapes. The VNA facilitates the connection of the two SMA connectors of the antenna prototype, enabling the measurement of the reflection coefficients of each port and the isolation coefficients between the two ports. Next, one port of the antenna is connected to a matching load, while the other port is linked to the VNA to quantify the radiation patterns of co-polarization and cross-polarization.

All the simulated and measured results are exhibited in Figure 4e-k and Figure S7. The dashed lines represent the simulated results, while the solid lines denote the measured results. In addition, due to the ultimately mirror-symmetric structure of the designed antenna, only the results for Port 1 input and Port 2 output are provided. Concerning SatCom scenarios, the range from 1.5 GHz to 1.7 GHz (the purple-shaded region in pictures) covers a particular communication frequency band that is specified by the GNSS including Global Positioning System (GPS), GLONASS, Galileo and BeiDou in the L-band. The reflection coefficient ($|S_{11}|$) in Figure 4e together with the isolation coefficient ($|S_{12}|$) in Figure 4f show that the frequency range with $|S_{11}|$ and $|S_{12}|$ less than -10 dB covers 1.5 GHz to 1.7 GHz, manifesting that the sum of the reflection to the input port and the output from another port is fewer than 10% of the total power fed in. Left-hand circular polarization (LHCP) is the co-polarization while Port 1 is excited. The axial ratio and realized broadside gain of the proposed antenna are shown in Figure 4g, h respectively. It is obvious that the antenna has a satisfactory axial ratio of less than 3 dB, and the bandwidth of a 1 dB decrease contains the required band with a low RHCP (cross-polarization) level, indicating that the proposed antenna possesses adequate CP properties. Meanwhile, two radiation nulls are located at 1.0 GHz and 2.1 GHz near the passband, with a suppression level of more than 30 dB. Besides these, in an effort to display the directionality of the antenna, the simulated three-dimensional (3-D) radiation patterns of LHCP and RHCP are illustrated in Figure S7, and several corresponding sectional normalized radiation patterns at 1.5 GHz, 1.6 GHz and 1.7 GHz are visualized in Figure 4i-k. The antenna beams power towards the upper half free space with similar pattern profiles between the xoz plane and the yoz plane, and maintains a desirable cross-polarization level with a co-polarization peak gain of up to 7.5 dBic. The slightly lower aperture efficiency of the proposed antenna is mainly due to the excessive loss of PDMS dielectric layers, as shown in Figures S8, S9, and S10, the radiation efficiency of the GAF-based antenna will be increased from 60% to more than 85% if the substrates are lossless. Errors in prototype fabrication and interference from the testing environment produce discrepancies between simulated and measured results.

To demonstrate the favourable performance of the proposed antenna, some selected indicators of the proposed GAF-based antenna with other reported CP antennas for SatCom applications are compared in Table 2. The table reveals that the designed metasurface antenna not only achieves a wide bandwidth coverage and satisfactory gain while maintaining a small profile of 0.021 λ_0, but also possesses additional FR characteristics. It is also noted that the intrinsic flexibility, anti-corrosion, mechanical stress resistance and environmental friendliness properties of our GAFs surpass those of reported traditional metal-based materials.

Table 2. Comparison with previous CP antennas

Ref.	CP Method	Profile (λ_0)	Operating Frequency (GHz)	$\lvert S_{11}\rvert$ BW (%)	ARBW (%)	Peak Gain (dBic)	FR properties
[39]	Patch with shorted parasitic stripes	0.016	1.57~1.58	1.7	0.63	5.4	No
[40]	Four-port 90° shifted divider	0.06	1.15~2.00	72.5	54.0	3.4	No
[41]	AMC loaded crossed dipole	0.11	1.25~1.97	66.3	44.7	6.0	No
[42]	Patch with annular parasitic ground strip	0.02	1.18~1.24 1.50~1.55	32.7	4.1 6.5	2.5 3.4	No
[43]	Quasi-symmetric crossed slots	0.16	1.07~1.65	43.8	42.6	6.3	No
[44]	Orthogonal modes of a dielectric resonator	0.22	1.37~2.04	38.8	39.4	7.8	Yes
This work	Metasurface excited by orthogonal slots	0.021	1.50~1.70	15.8	27.8	7.5	Yes

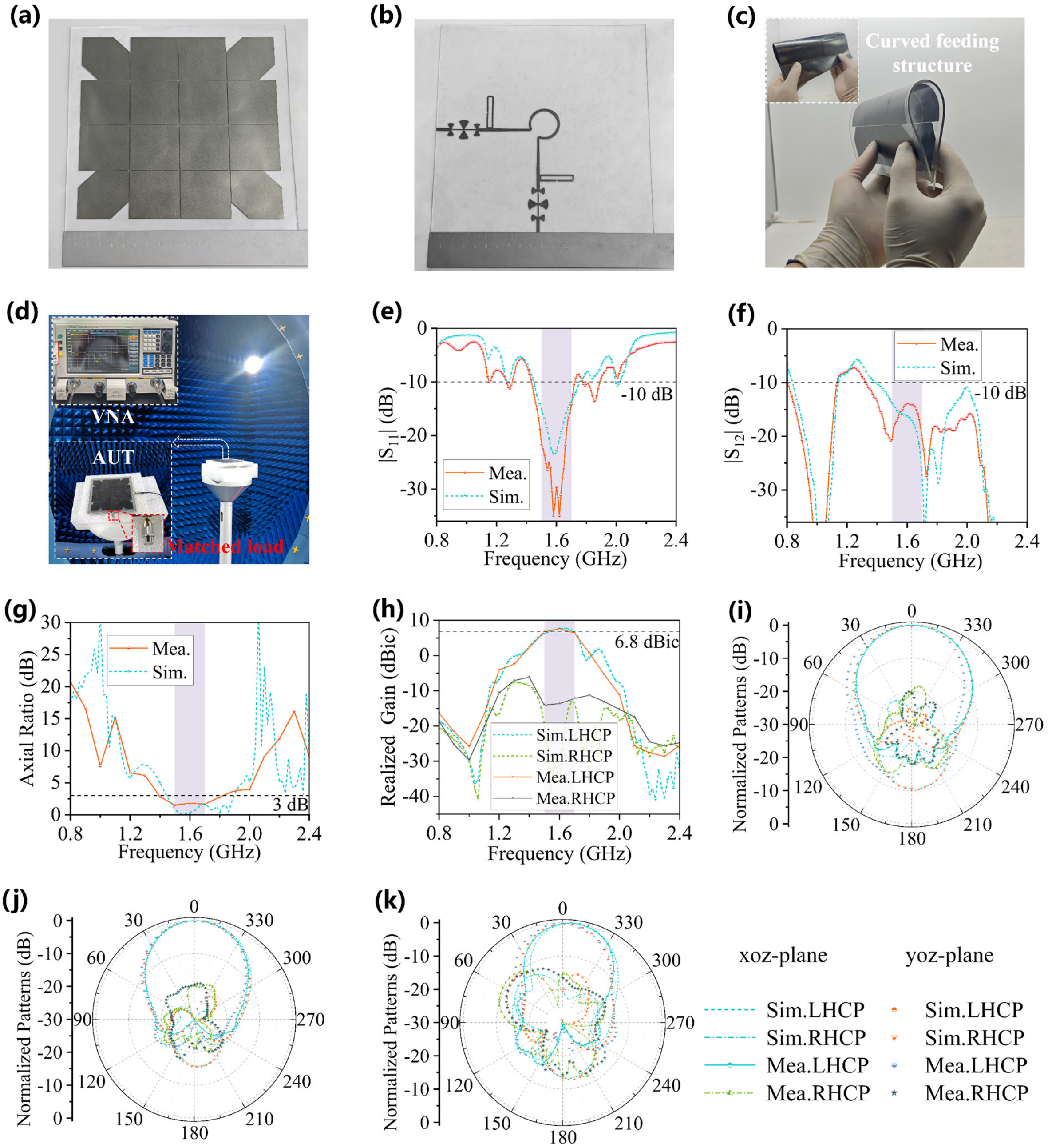

Figure 4. Performance of the proposed GAF antenna. (a) Prototype of the metasurface affixed on PDMS substrate. (b) Prototype of the feeding microstrip line. (c) Bent metasurface and feeding structures. (d) Multi-probe dual-polarization antenna measurement system. (e) Reflection coefficient. (f) Isolation coefficient. (g) Axial ratio. (h) Realized gain. Normalized gain patterns at (i) 1.5 GHz, (j) 1.6 GHz and (k) 1.7 GHz.

3.4 Anti-corrosion and flexibility properties

The oxidation to corrosion of the antenna leads to a substantial amount of inhomogeneous adhered media on the surface, thereupon then affecting the transmission efficiency and reception quality of the wireless signals. Besides, the physical intensity of the antenna is weakened, and the structure is prone to damage to pose a threat to the stable operation of the communication system.

To confirm the excellent corrosion resistance and flexibility of the GAF-based antenna, salt spray and bending experiments are conducted separately on various structures of the proposed GAF antenna. During the salt spray test, we use a sprinkling bottle to uniformly sprinkle sodium chloride (NaCl) solution with a mass fraction of 5% twelve times a day, and then all experimental samples are placed in an unpolluted fume hood. The record data from samples of spray disposition are rinsed with water to remove the thick NaCl crystals on their surface, some pictures before the washing procedure are shown in Figures S11 and S12.

Figure 5a-d shows the distinction in corrosion resistance characteristics of GAF and copper foil. Specifically, Figure 5a and Figure 5c depict the original appearance of patterns made of GAFs and copper foils derived from the proposed antenna, respectively. It can be noticed that the metasurface pattern of two different materials is precisely manufactured, and there are no evident signs of corrosion or oxidation on either of their burnished surfaces. However, after undergoing five days of salt spray treatment, a large number of significant indications of oxidation appear on patterns fabricated by copper foil, such as a blue colour that represents the generation of copper ion compounds, as well as black oxidation products on the surface. In contrast, there is no occurrence of corrosion on GAF-based patterns even suffered twenty days of salt spray deposition. Indicating that GAF possesses superior corrosion prevention ability and antioxidant performance in comparison to copper.

Figure 5e-h presents the outcomes of bend testing results performed on GAF and copper foil. Remarkably, after being subjected to fifty thousand rounds of 90° bending, only a few wrinkles arose on the surface of the GAF-based antenna patterns, with their structures remaining intact without mechanical damage. In stark contrast, copper foil patterns showed significant fracture and deformations after just a thousand times bending, with the feeding line dehiscing in the corners and LPF narrow structure, as evidenced in Figure 5g and Figure 5h. For accurately designed and manufactured antennae in communication systems, cracking can prominently impede the proper functionality of the antenna, underscoring the excellent bending resistance characteristics of GAF compared to copper foil.

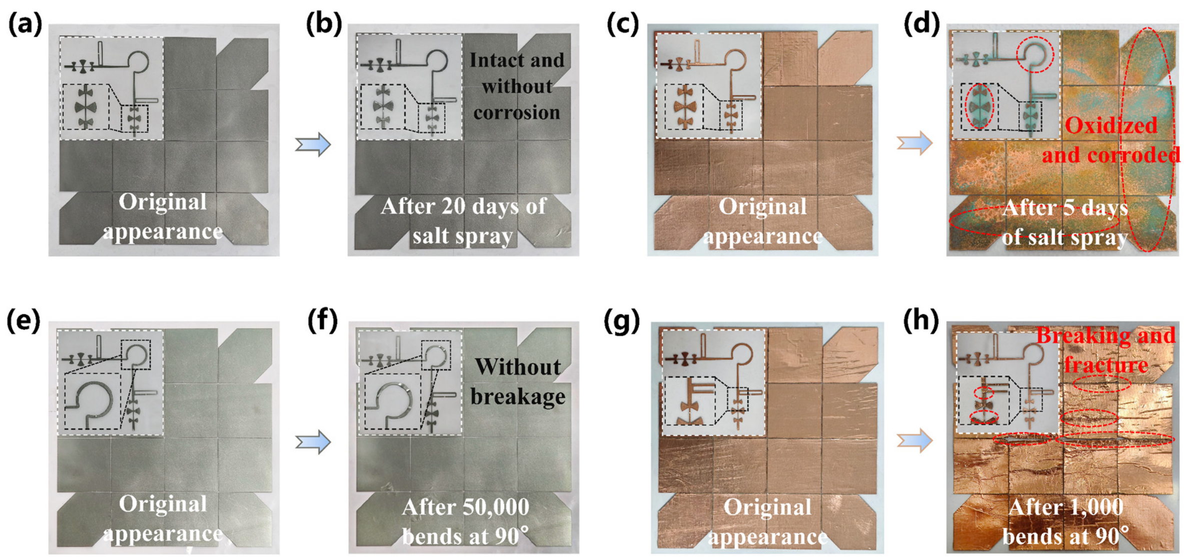

Figure 5. Comparison of anti-corrosion and bending resistance properties between GAF patterns and copper foil patterns. GAF-based metasurface pattern and feeding network, (a) before salt spray treatment. (b) after twenty days of salt spray. Metasurface pattern and feeding structure, (c) before salt spray treatment. (d) under five days of salt spray. (e) GAF patterns before bending and (f) suffer 90° bending for fifty thousand times. (g) Copper foil patterns before bending and (h) after experiencing a thousand times bends for 90°.

In many previously reported works, metal-based antennas corroded [33, 45] or damaged by mechanical bending [46] are prone to function inadequacies, which is largely due to the irregular deformations and fractures that emerge as a result of a large number of discontinuous structures. These undesirably structure formations, as has been observed in Figure 5, tend to augment the energy reflection and shift the operating frequency of the antennas, eventually rendering them inoperable. On the contrary, GAF-based antennas demonstrate their strong anti-corrosion characteristics and mechanical bending resistance. Moreover, the lightweight, foldable and environmentally friendly properties of GAFs will bring more possibilities for SatCom applications.

4. Conclusion

A dual-CP metasurface antenna for SatCom application based on high conductivity GAFs has been proposed. Inspired by the critical issue of poor flexibility and susceptibility to oxidation and corrosion in traditional metal materials. The GAFs with a conductivity of up to 1.13×10^6 S/m are utilized for the fabrication of RF electronic devices. Using PDMS as substrates for antenna design and manufacturing to achieve desirable flexibility characteristics. Simulation and measurement results show excellent performance of the proposed antenna. By building sequentially rotating slot lines for near-field coupling of EM energy to a 4×4 metasurface patch, combining with a mirror-symmetric microstrip feeding line to materialize wideband dual-CP. The LPF and SRR structures are employed to guarantee the out-of-band suppressions outside the L-band. Additionally, salt spray and mechanical bending experiments in comparison with copper foil further prove the exceptional oxidation prevention, anti-corrosion and bending resistance characteristics of GAFs. Overall, these outstanding properties make the proposed GAF-based antenna the preferred candidate for SatCom applications.

ASSOCIATED CONTENT

Supporting Information

Pictures of antenna prototype elements; Simulated 3-D radiation patterns; Antenna measurement system; NaCl crystallization on the surface of copper and GAF metasurface pattern.

AUTHOR INFORMATION

Corresponding Authors

Haoran Zu - Hubei Engineering Research Center of RF-Microwave Technology and Application, Wuhan University of Technology, Wuhan 430070, China & School of Information Engineering, Wuhan University of Technology, Wuhan 430070, China
Jie Shen - Hubei Engineering Research Center of RF-Microwave Technology and Application, Wuhan University of Technology, Wuhan 430070, China
Daping He - Hubei Engineering Research Center of RF-Microwave Technology and Application, Wuhan University of Technology, Wuhan 430070, China

Authors

Zhi Luo - Hubei Engineering Research Center of RF-Microwave Technology and Application, Wuhan University of Technology, Wuhan 430070, China
Peng Li- Hubei Engineering Research Center of RF-Microwave Technology and Application, Wuhan University of Technology, Wuhan 430070, China
Yitong Xin - Hubei Engineering Research Center of RF-Microwave Technology and Application, Wuhan University of Technology, Wuhan 430070, China
Qian Wei - Hubei Engineering Research Center of RF-Microwave Technology and Application, Wuhan University of Technology, Wuhan 430070, China
Bilei Zhou - Air Force Early Warning Academy, Wuhan 430019, China
Rongguo Song - Hubei Engineering Research Center of RF-Microwave Technology and Application, Wuhan University of Technology, Wuhan 430070, China & Air Force Early Warning Academy, Wuhan 430019, China

Acknowledgements

The authors acknowledge financial support from the National Natural Science Foundation of China (51672204, 51701146) and Foundation of the National Key Laboratory of Microwave Imaging Technology and supported by the Fundamental Research Funds for the Central Universities (WUT: 2024IVA031). We also thank the Analytical and Testing Center of Wuhan University of Technology for performing various characterization and measurements.

Notes

The authors declare that they have no known competing financial interests or personal

relationships that could have appeared to influence the work reported in this paper.

References

(1) Shen, L., Jacob, D.J., Gautam, R. et al. National quantifications of methane emissions from fuel exploitation using high resolution inversions of satellite observations. Nat. Commun. 2023, 14, 4948.

(2) Randy, S. Landsat 9 Satellite Continues Half-Century of Earth Observations: Eyes in the sky serve as a valuable tool for stewardship. BioSci. 2022, 72, 226-232.

(3) Claudio, S.; Abbas, J.; Marina, R. Aerospace Communications and Networking in the Next Two Decades: Current Trends and Future Perspectives. Proc. IEEE 2011, 99, 1835-1839.

(4) Xiao, Z. Y.; Han, Z.; Nallanathan, A.; A. Dobre, O.; Clerckx, B.; Choi, J.; He, C.; Tong, W. Guest Editorial Special Issue on Antenna Array Enabled Space/Air/Ground Communications and Networking. IEEE J. Sel. Areas Commun. 2022, 40, 2767-2772.

(5) Li, B. S.; Zhou, L.; Qin, J. H.; Zhou, T. J.; Chen, D. K.; Hou, S. G.; Murthgudde, R. Middle east warming in spring enhances summer rainfall over Pakistan. Nat. Commun. 2023, 14, 7635.

(6) Seabrook, S.; Mackay, K.; Watson, S. J.; Clare, M. A.; Hunt, J. E.; Yeo, I. A.; Lane, E. M.; Clark, M. R.; Wysoczanski, R.; Rowden, A. A.; Kula, T.; Hoffmann, L. J.; Armstrong, E. & Williams, M. J. M. Volcaniclastic density currents explain widespread and diverse seafloor impacts of the 2022 Hunga Volcano eruption. Nat. Commun. 2023, 14, 7881.

(7) Wang, Y.; Yan, C.; Cheng, S.; Xu, A.; Sun, X. P.; Xu, Y.; Chen, J.; Jiang, Z.; Liang, K.; Feng, Z. Flexible RFID Tag Metal Antenna on Paper-Based Substrate by Inkjet Printing Technology. Adv. Funct. Mater. 2019, 29, 1902579.

(8) Zu, H.; Wu, B.; Su, T. Beam Manipulation of Antenna With Large Frequency-Scanning Angle

Based on Field Confinement of Spoof Surface Plasmon Polaritons. IEEE Trans. Antennas Propag. 2022, 70, 3022-3027.

(9) Chen, B.; Wu, B.; Zu, H.; Hou, J.; Su, T. Experimental Demonstration of High Optically Transparent Reflectarrays Using Fine Metal Line Structure. IEEE Trans. Antennas Propag. 2022, 70, 10504-10511.

(10) Zhao, Y.; Zhang, T.; Xiong, H.; Wang, F. Bridge for the thermodynamics and kinetics of electrochemical corrosion: Modeling on dissolution, ionization, diffusion and deposition in metal/solution interface. Corros. Sci. 2021, 191, 109763.

(11) Boda, U.; Strandberg, J.; Eriksson, J.; Liu, X. J.; Beni, V.; Tybrandt, K. Screen-Printed Corrosion-Resistant and Long-Term Stable Stretchable Electronics Based on AgAu Microflake Conductors. ACS Appl. Mater. Interfaces. 2023, 15, 12372-12382.

(12) Asci, C.; Sadeqi, A.; Wang, W.; Rezaei Nejad, H.; Sonkusale, S. Design and implementation of magnetically-tunable quad-band filter utilizing split-ring resonators at microwave frequencies. Sci. Rep.-UK 2020, 10, 1050.

(13) Kaim, V.; Kanaujia, B. K.; Kumar, S.; Choi, H. C.; Kim, K. W.; Rambabu, K. Ultra-Miniature Circularly Polarized CPW-Fed Implantable Antenna Design and its Validation for Biotelemetry Applications. Sci. Rep.-UK 2020, 10, 6795.

(14) Badeenezhad, A.; Soleimani, H.; Shahsavani, S.; Parseh, I.; Mohammadpour, A.; Azadbakht, O.; Javanmardi, P.; Faraji, H.; Nalosi, K. B. Comprehensive health risk analysis of heavy metal pollution using water quality indices and Monte Carlo simulation in R software. Sci. Rep.-UK 2023, 13, 15817.

(15) Li, Y.; Dong, Z.; Feng D.; Zhang, X.; Jia, Z.; Fan, Q.; Liu, K. Study on the risk of soil heavy metal pollution in typical developed cities in eastern China. Sci. Rep.-UK 2022, 12, 3855.

(16) Cai, C. Z.; Huertas, A. D.; Agusti, S. Declining nutrient availability and metal pollution in the Red Sea. Commun. Earth & Environ. 2023, 4, 424.

(17) Song, R.; Jiang, S.; Hu, Z.; Fan, C.; Li, P.; Ge, Q.; Mao, B.; He, D. Ultra-high conductive graphene assembled film for millimeter wave electromagnetic protection. Sci. bull. 2022, 67, 1122-1125.

(18) Song, R.; Wang, Z.; Zu, H.; Chen, Q.; Mao, B.; Wu, Z. P.; He, D. Wideband and low sidelobe graphene antenna array for 5G applications. Sci. bull. 2021, 66, 103-106.

(19) Song, H.; Jeon, H.; Im, D.; Çakmakçı, N.; Shin, K.; Jeong, y. Free-standing carbon nanotube film for high efficiency monopole antenna. Carbon. 2022, 187, 22-28.

(20) Puchades I., Rossi J. E., Cress C. D., Naglich E., and Landi B. J. Carbon Nanotube Thin-Film Antennas. ACS Appl. Mater. Interfaces. 2016, 8, 20986-20992.

(21) Gao, M.; Wang, B.; Yao, Y.; Taheri, M.; Wang, P.; Chu, D.; Lu, Y. Carbon nanotube thin film patch antennas for wireless communications. Appl. Phys. Rev. 2023, 10, 203102.

(22) Han, M.; Liu, Y.; Rakhmanov, R.; Israel, C.; Tajin, M. A. S.; Friedman, G.; Volman, V.; Hoorfar, A.; Dandekar, K. R; Gogotsi, Y. Solution-Processed Ti3C2Tx MXene Antennas for Radio-Frequency Communication. Adv. Mater. 2021, 33, 2003225.

(23) Jun, J.; Oh, J.; Shin, D. H.; Kim, S. G.; Lee, J. S.; Kim, W.; Jang, J. Wireless, Room Temperature Volatile Organic Compound Sensor Based on Polypyrrole Nanoparticle Immobilized Ultrahigh Frequency Radio Frequency Identification Tag. ACS Appl. Mater. Interfaces. 2016, 8,

33139-33147.

(24) Zu, H.; Wu, B.; Zhang, Y.; Zhao, Y.; Song, R.; He, D. Circularly Polarized Wearable Antenna With Low Profile and Low Specific Absorption Rate Using Highly Conductive Graphene Film. IEEE Antenn. Wirel. Pr. 2020, 19, 2354-2358.

(25) Xiao, Y.; Zu, H.; Song, R.; Xin, Y.; Xi, Y.; Huang, G.; Wu, B.; He, D. Multiband and Low-Specific-Absorption-Rate Wearable Antenna With Low Profile Based on Highly Conductive Graphene Assembled Film, IEEE Antenn. Wirel. Pr. 2023, 5, 2195-2199.

(26) Okuda, R.; Niwano, K.; Hatada, K.; Kokubu, K.; Suga, R.; Watanabe, T.; Koh, S. Evaluation of transmission characteristics of CVD-grown graphene and effect of tuning electrical properties of graphene up to 50 GHz. Sci. Rep. -UK 2023, 13, 13878.

(27) Song, R.; Wang, Q.; Mao, B.; Wang, Z.; Tang, D.; Zhang, B.; Zhang, J.; Liu, C.; He, D.; Wu, Z.; Mu, S. Flexible graphite films with high conductivity for radio-frequency antennas. Carbon. 2018, 130, 164-169.

(28) Awan, S. A.; Lombardo, A.; Colli, A.; Privitera, G.; Kulmala, T. S.; Kivioja, J. M.; Koshino, M.; Ferrari, A.C. Transport conductivity of graphene at RF and microwave frequencies. 2D Mater. 2016, 3, 15010.

(29) Colmiais, I.; Silva, V.; Borme, J.; Alpuim, P.; Mendes, P. M. Towards RF graphene devices: A review. FlatChem. 2022, 35, 100409.

(30) Palacios, T.; Hsu, A.; Wang, H. Applications of graphene devices in RF communications. IEEE Commun. Mag. 2010, 48, 122-128.

(31) Colombo, L.; Wallace, R. M.; Ruoff, R. S. Graphene Growth and Device Integration. Proc.

IEEE 2013, 7, 1536-1556.

(32) Song, R.; Si, Y.; Qian, W.; Zu, H.; Zhou, B.; Du, Q.; He, D.; Wang, Y. Investigation of MXene nanosheets based radio-frequency electronics by skin depth effect. Nano Res. 2023.

(33) Song, R.; Mao, B.; Wang, Z.; Hui, Y.; Zhang, N.; Fang, R.; Zhang, J.; Wu, Y.; Ge, Q.; Novoselov, K. S.; He, D. Comparison of copper and graphene-assembled films in 5G wireless communication and THz electromagnetic-interference shielding. PNAS. 2023, 120, e2085160176.

(34) Ray, M. K.; Mandal, K.; Nasimuddin, N. Low Profile Circularly Polarized Patch Antenna with Wide 3-dB Beamwidth. IEEE Antenn. Wirel. Pr. 2019, 18, 2473-2477.

(35) Chen, Z. N.; Qing, X.; Su, Y.; Xu, R. Toward Metantennas: Metamaterial-Based Antennas for Wireless Communications. IEEE Commun. Mag. 2023, 61, 160-165.

(36) Zu, H.; Wu, B.; Chen, B; Li, W.; Su, T.; Liu, Y.; Tang, W.; He, D. P.; Cui, T. Optically and radiofrequency-transparent metadevices based on quasi-one-dimensional surface plasmon polariton structures. Nat. electron. 2023, 6, 525-533.

(37) Luo, W.; Yan, S.; Zhou, J. Ceramic-based dielectric metamaterials. Interdiscip. Mater. 2022, 1, 11-27.

(38) Chen, J.; H, S.; Zhu, S.; Li, T. Metamaterials: From fundamental physics to intelligent design. Interdiscip. Mater. 2023, 2, 5-29.

(39) Wang M. S., Zhu X. Q., Guo Y. X. Compact Circularly Polarized Patch Antenna With Wide Axial Ratio Beamwidth. IEEE Antenn. Wirel. Pr. 2018, 17, 718–714.

(40) Wang L., Wen Z. B., Jiao Y. C., Zhang W. J., Zhang C. A Low Profile Broadband Circularly

Polarized Microstrip Antenna With Wide Beamwidth. IEEE Antenn. Wirel. Pr. 2018, 17, 1213–1217.

(41) Feng D., Zhai H. Q., Xi L., Yang S., Zhang K. D., Yang D. A Broadband Low-Profile Circular-Polarized Antenna on an AMC Reflector. IEEE Antenn. Wirel. Pr. 2017, 16, 2840–2843.

(42) Liu H. M., Chen C. H., Wang Z. B. Beamwidth-Enhanced Low-Profile Dual-Band Circular Polarized Patch Antenna for CNSS Applications. International Journal of Antennas and Propagation. 2019, 7630815.

(43) Zhang H. L., Guo Y. Y., and Wang G. A Wideband Circularly Polarized Crossed-Slot Antenna With Stable Phase Center. IEEE Antenn. Wirel. Pr. 2019, 18, 941–945.

(44) Qian Y., Xie S. Wideband Circularly Polarized Filtering Hybrid Antenna. Appl. Sci. 2022, 12, 11018.

(45) Hui Y. Y., Zu H. R., Song R. G, Fu H. Q., Luo K. L., Tian C., Wu B., Huang G., Kou Z. K., Cheng X., and He D.P. Graphene-assembled film-based reconfigurable filtering antenna with enhanced corrosion-resistance. Crystals, 2023, 13, 747.

(46) Ye D., Zu H., Hu Z. L., Xin Y. T., Guo J. N., Song R. G., He D. P. Flexible and Compact Tri-Band Graphene Antenna for Conformal Wi-Fi/WiMAX/5G Applications. IEEE Transactions on Circuits and Systems II: Express Briefs. 2023, 71, 1086-1090.

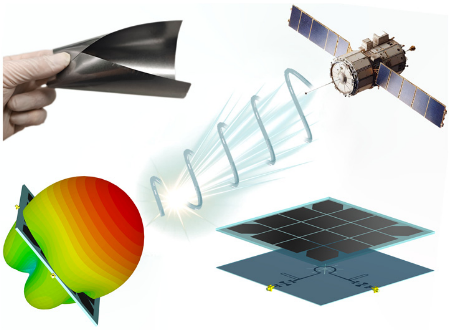

Table of Contents graphic